RSC Advances

PAPER

View Article Online
View Journal | View Issue

Cite this: *RSC Adv.*, 2026, **16**, 15709

Performance-optimized N-doped $CrCo_2O_4$ nanoferrite integrated with CNTs: a high-performance photocatalyst for next-generation wastewater remediation

Mohamed Abdel Rafea,[a] Kashif Ali,[b] Mohamed I. Attia,[c] M. M. Rashed,[a] Mohamed R. El-Aassar,[d] Imran Shakir,[e] Abdullah K. Alanazi,[f] Sidra Mubeen*[g] and Muhammad Aadil *[h]

Photocatalysis offers a scalable route to safeguard water security by destroying persistent dyes and drug residues under sunlight. We report a dual-strategy enhancement of spinel chromium cobaltite ($CrCo_2O_4$, CCO) *via* nitrogen doping (NCCO) and carbon-nanotube (CNT) compositing (NCCO@CNTs), synthesized by wet-chemical precipitation (urea as N source) followed by ultrasonication with CNTs. XRD/FTIR confirm phase-pure spinel formation with N-induced lattice disorder; SEM/EDX show improved dispersion and homogeneous N/Cr/Co/O/C distribution; UV-Vis/Tauc reveal band-gap narrowing from ~3.0 eV (CCO) to ~2.65 eV (NCCO); transient photocurrent demonstrates possible effective charge separation in NCCO@CNTs. Under natural sunlight (7 ppm, 25 mg catalyst, 75 mL), NCCO@CNTs degrades methylene blue (MB) and amoxicillin (AMX) by 90.7% and 85% in 60 min, surpassing NCCO (65.7%, 62%) and CCO (49.5%, 47.5%). Pseudo-first-order kinetics yield rate constants k(MB) = 0.037, 0.017, 0.011 min^{-1} and k(AMX) = 0.030, 0.015, 0.010 min^{-1} for NCCO@CNTs, NCCO, and CCO, respectively (≥3× over pristine CCO). Radical-trapping pinpoints $^{\bullet}O_2^-$ and $^{\bullet}OH$ as dominant species, aligning with a mechanism wherein N-doping broadens visible-light absorption/creates shallow states, while CNTs act as rapid electron sinks, suppressing e^-/h^+ recombination and adding adsorption/active sites. Benchmarking against reported spinel's indicates competitive or superior sunlight activity. By optimizing the performance of $CrCo_2O_4$ through dual modification (nitrogen doping and CNT compositing), this work enhances its photocatalytic activity, enabling effective degradation of a wide range of chemically distinct pollutants, and offers a scalable solution for practical wastewater remediation.

Received 11th November 2025
Accepted 20th February 2026

DOI: 10.1039/d5ra08692b

rsc.li/rsc-advances

1. Introduction

In developing countries with a rapid increase in population, there is a severe issue with the environmental consequences of waste produced by the newly established industries. Many organic contaminants, such as dyes and synthetic drugs, are toxic to aquatic life and threaten human life.[1,2] Discharged industrial waste products, antibiotics, and synthetic dyes contribute to water pollution and waterborne diseases. Over 750 million people need protection from drinking contaminated water, and their numbers are still increasing. More than 97 percent of the water present on Earth is salty, which means only 2 percent of the water is usable and safe to drink.[3] Approximately 10% of all dyes released into the environment are attributed to wastewater produced by the industrial sectors. Synthetic dyes and antibiotics are of special attention among these pollutants because of their persistence, toxic effects, and high detection rates in aquatic systems.[4]

Organic dyes like methylene blue and Rh–B dyes are widely used in the textile, paper, and cosmetic industries, as well as in the pharmaceutical industry. Although intended and valuable for their desired purposes, these dyes are well known for their photochemical and biodegradation stability. When discharged

[a]*Department of Physics, College of Science, Imam Mohammad Ibn Saud Islamic University (IMSIU), 11623, Riyadh, Saudi Arabia*
[b]*Division of Science and Technology, Department of Zoology, University of Education, Lahore, Pakistan*
[c]*Department of Chemistry, College of Science, Imam Mohammad Ibn Saud Islamic University (IMSIU), 11623, Riyadh, Saudi Arabia*
[d]*Chemistry Department, College of Science, Jouf University, Sakaka, 2014, Saudi Arabia*
[e]*Department of Physics, Faculty of Science, Islamic University of Madinah, Madinah 42351, Saudi Arabia*
[f]*Department of Chemistry, College of Science, Taif University, Taif, Saudi Arabia*
[g]*Department of Chemistry, The Women University, Multan, 60000, Pakistan. E-mail: Sidra.mubeen@wum.edu.pk*
[h]*Department of Chemistry, Rahim Yar Khan Campus, The Islamia University of Bahawalpur, Rahim Yar Khan 64200, Pakistan. E-mail: Muhammad.aadil@iub.edu.pk*

into water bodies, they are long-lasting, bringing adverse effects to waterborne organisms.[5] For instance, methylene blue may reduce light penetration in aquatic plants and consequently lead to low oxygen levels to the extent that plant and animal structures in the water adjust and finally die off. Environmental degradation has become an inevitable consequence of the fast economic and technological progress in recent decades. Antibiotics like levofloxacin, ciprofloxacin, amoxicillin, and tetracycline have become major environmental pollutants because of their usage in human and veterinary medicine.[6–8] These antibiotics are anticipated to provide sufficient and potent inhibition against bacteria, hence their usage in treating bacterial infections. However, due to misuse and inadequate discharging of these antibiotics, they have been found to precipitate in various compartments in the environment, such as rivers, lakes, and groundwater.[9,10]

Photocatalysis has become a substantial technique for the catalytic decomposition of organic pollutants, including drugs, dyes, pesticides, *etc.* The efficiency of the photocatalytic processes mainly depends on the performance of the photocatalyst, but challenges persist in achieving stable light-to-electron conversion.[11] Semiconductor materials are widely utilized for the degradation of antibiotic contaminants and organic dyes in wastewater due to their cost-efficiency, stable nature, tunable band gaps, variable oxidation states, and extended absorption spectra, enabling efficient photocatalytic activity. TiO_2, SnO_2, PbO_2 and ZnO are frequently employed in photocatalytic applications.[12] Despite the widespread utilization of these photocatalysts, their photocatalytic activity diminishes over time due to certain recurrent flaws. The key flaws are the poor separation of charge carriers, rapid recombination of charge carriers, too large band gap, and the need for UV light to excite electrons. All of these aspects add up to reducing their overall efficiency, constraining their practical applications, and rendering them less appropriate for sustainable environment purification.[13]

The AB_2O_4 spinel framework—hosting a divalent A cation and trivalent B cation—supports broad functionality in photocatalysis, energy devices, and sensing due to its adaptable structure.[14,15]

The cobalt chromite, $CrCo_2O_4$, a prominent member of the spinel structured semiconductive material used extensively in catalytic applications. Using controlled, position-specific partial doping—swapping Cr^{2+} and Co^{3+} at octahedral and tetrahedral sites with suitable metal or non-metal dopants—one can systematically tailor electronic and optical responses, thereby upgrading the material's photocatalytic efficacy.[16] However, native $CrCo_2O_4$ tends to show limited visible-light absorption, insufficient charge separation, and fast recombination. Remedies include nitrogen doping and composite design; N-doping narrows the band gap and introduces controlled defects that help separate carriers.[17]

Carbon nanotubes (CNTs), when reinforced with the semiconductive photocatalytic materials, act as co-catalysts and strengthen the photocatalyst in three complementary ways:[18,19] Firstly, being extremely conductive, it raises electrical conductivity of the resultant composite, hence promoting charge transport. Secondly, owing to its larger specific surface area and one-dimensional structure feature, it gets entangled with semiconductive material particles and suppresses their agglomeration, which results in it furnishing abundant active sites to adsorb pollutants, boosting degradation rates. Thirdly, being a carbonaceous material, it exhibits a broad optical absorption range; hence, on reinforcing with semiconductive material, it can improve solar light harvesting and overall activity.[20,21] Synergism is realized by introducing nitrogen doping and CNT composite development, which addresses the shortcomings of $CrCo_2O_4$ and substantially enhances its photocatalytic performance for environmental cleaning.

Here in the current study, we have prepared chromium cobaltite ($CrCo_2O_4$, CCO) and nitrogen-doped chromium cobaltite (N-$CrCo_2O_4$, NCCO) through wet chemical method. The N-$CrCo_2O_4$@CNTs composite was prepared using an ultrasonication approach, which allowed suitable distribution of carbon nanotubes (CNTs) into the nitrogen doped spinel structure. The prepared materials were characterized in detail to confirm the integrity of their structure, morphology and composition using XRD, SEM, EDX and FTIR. The optical and opto-electronic properties of the materials were also studied to examine their feasibility for photocatalytic applications. The synergistic effects of N-doping and CNT composite formation were investigated for the photocatalytic activity of the prepared NCCO@CNTs by degrading two different pollutants in water, one arising from textile (methylene blue dye) and another from pharmaceutical industries (amoxicillin). These pollutants were chosen to mimic complex, multi-pollutant polluted water, indicating that the resulting products have potential applications for wider treatment of contaminated water.

2. Experimental section

2.1 Chemicals required

The details regarding the chemicals used for the synthesis of CCO, NCCO, and NCCO@CNTs, as presented in Table 1.

2.2 Synthesis of CCO, NCCO, and NCCO@CNTs

Chromium cobaltite ($CrCo_2O_4$, CCO) was synthesized through a wet chemical method. A solution of $Co(NO_3)_2 \cdot 6H_2O$ and $Cr(NO_3)_3 \cdot 9H_2O$ in a 2 : 1 molar ratio was dissolved in 150 mL of deionized water. To adjust the pH to 11, a 2.0 M NaOH solution (50 mL) was added dropwise. The mixture was agitated for 30 min until a dark green colour developed and precipitates formed. The reaction mixture was then washed well several times with double-distilled water after precipitation to neutralize and eliminate excessive by-products of reactants. The precipitate was collected and dried in an oven at 100 °C for 12 h and annealed at 400 °C for another 4 h in furnace to crystallize. The CCO product obtained was observed as dark green powder.

The synthesis of nitrogen-doped chromium cobaltite was realized in a similar manner to CCO, with urea added to the solution at the beginning of the procedure, as given in Fig. 1 (step-I). Urea served as a source of nitrogen to enter its atoms into the spinel frame and thereby change its properties, making

Table 1 List of chemicals used in the synthesis of CCO, NCCO, and NCCO@CNTs, including their formulas, purity, and supplier information

S. no.	Name	Formula	Purity	Supplier
1	Cobalt nitrate hexahydrate	$Co(NO_3)_2 \cdot 6H_2O$	99%	Sigma-Aldrich
2	Chromium nitrate	$Cr(NO_3)_3 \cdot 9H_2O$	99%	Sigma-Aldrich
3	Deionized water	H_2O	—	Sigma-Aldrich
4	Urea	$CO(NH_2)_2$	99%	Sigma-Aldrich
5	Sodium hydroxide	NaOH	98%	Sigma-Aldrich
6	Carbon nanotubes (dispersed)	CNTs	5–10 mg L^{-1}	Sigma-Aldrich

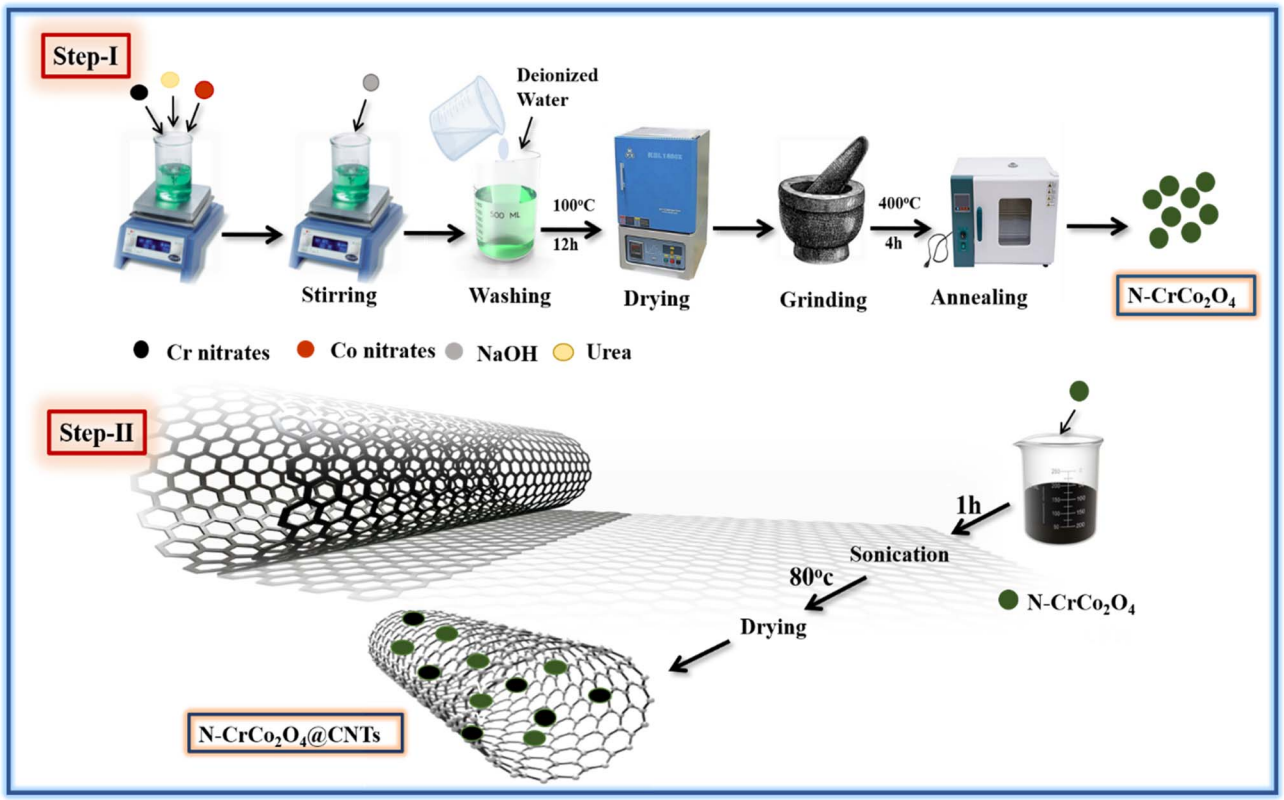

Fig. 1 Steps involved in the synthesis of NCCO and NCCO@CNTs composite.

it more suitable to be a photocatalyst. The composite sample containing NCCO and CNTs was then prepared by adopting well know ultrasonication methodology. The weight % of the NCCO and CNTs were kept 85% and 15% respectively. The NCCO and CNTs were dispersed in water and sonicated the suspension of 1 hour at 80 °C, as shown in Fig. 1 (step-II). Then, the water was slowly evaporated by keeping the predeparture below the boiling point of water and solid composite sample was achieved.

2.3 Evaluation of photocatalytic degradation

Two different organic pollutants, *i.e.*, methylene blue (MB) dye commonly existing in the textile effluents and the amoxicillin drug commonly existing in the pharmaceutical pollutants, were used to examine and compare the photocatalytic aptitude of the CCO, NCCO, and NCCO@CNTs. The photocatalytic experiment was performed under natural sunlight on the RYK sub-campus of Islamic University of Bahawalpur, Pakistan; solar irradiance was in the range of 585 to 602 W m^{-2} (Kipp & Zonen Pyranometer CMP-11). The temperature varied between 25–33 °C. A UV-cutoff filter was used to exclude wavelengths below 380 nm, ensuring visible-light-driven photocatalysis. For these experiments, 25 mg of fabricated photocatalysts was dispersed in 75 mL solutions containing 7 ppm concentrations of MB dye and amoxicillin. Initially, the solutions were magnetically stirred in the dark for 45 minutes to establish adsorption–desorption equilibrium. At predetermined intervals of 10 minutes, 4 mL samples were withdrawn from the reaction mixture, centrifuged at 4000 rpm to separate the photocatalysts, and analyzed using a UV-Vis spectrophotometer. The absorbance of MB dye was measured at 668 nm, while amoxicillin was measured at 230 nm. The degradation efficiency of the photocatalysts was calculated using eqn (1):[22]

$$\% \text{ Degradation} = 1 - \frac{A_t}{A_0} \times 100 \quad (1)$$

where A_0 represents the initial absorbance of the dye or antibiotic, and A_t corresponds to the absorbance measured at a given time t. The degradation rate constant k was determined by eqn (2):[23]

$$-\ln\left[\frac{A_t}{A_0}\right] = kt \quad (2)$$

This method allows for a comprehensive evaluation of the photocatalytic performance of NCCO and NCCO@CNTs for degrading different concentrations of organic pollutants, contributing to their evaluation for environmental applications.

3. Result and discussion

3.1 Structural analysis

The powder X-ray diffraction (XRD) patterns of CCO, NCCO, and NCCO@CNTs, obtained using a Shimadzu 6100AS, are given in Fig. 2a. The X-ray diffraction pattern of CCO had the following peaks at selected 2θ values in terms of Miller indices (*hkl*), *viz.*, (220) 30.67°, (311) 36.17°, (222) 37.88°, (400) 44.7°, (422) 55.0°, (511) 58.42°, 3, (440) 64.5°, and (533) 76.6°. All eight peaks are in good agreement with JCPDS 00-024-0326,[24] hence ensuring the successful synesis of $CrCo_2O_4$ with cubic spinel phase.

The sharpness of the diffraction peaks ensures the satisfactory crystallinity, while the nonexistence of any irrelevant peak ensures the purity of the prepared CCO. In NCCO, even after N-doping, no additional diffraction peaks were detected. Nevertheless, one can observe three prominent differences in the diffraction pattern that occurs following N-doping. First, a decrease in peak intensity was noticed. This weakened intensity may result from the lattice defects and disorder introduced by N doping. These defects disrupt the regular atomic arrangement, scattering X-rays and lowering the diffraction signal. Second, a small shift towards the higher 2θ values was found meaning that lattices have shrunk owing to smaller nitrogen atoms than larger ones being replaced and *d*-spacing were reduced which lead diffraction peaks shifting to higher angles. Third, a broadening of the peaks was also found in NCCO XRD pattern indicating some structural disorder due to the introduction of nitrogen. The broadening of FWHM can be attributed to smaller crystallite sizes, which is caused by

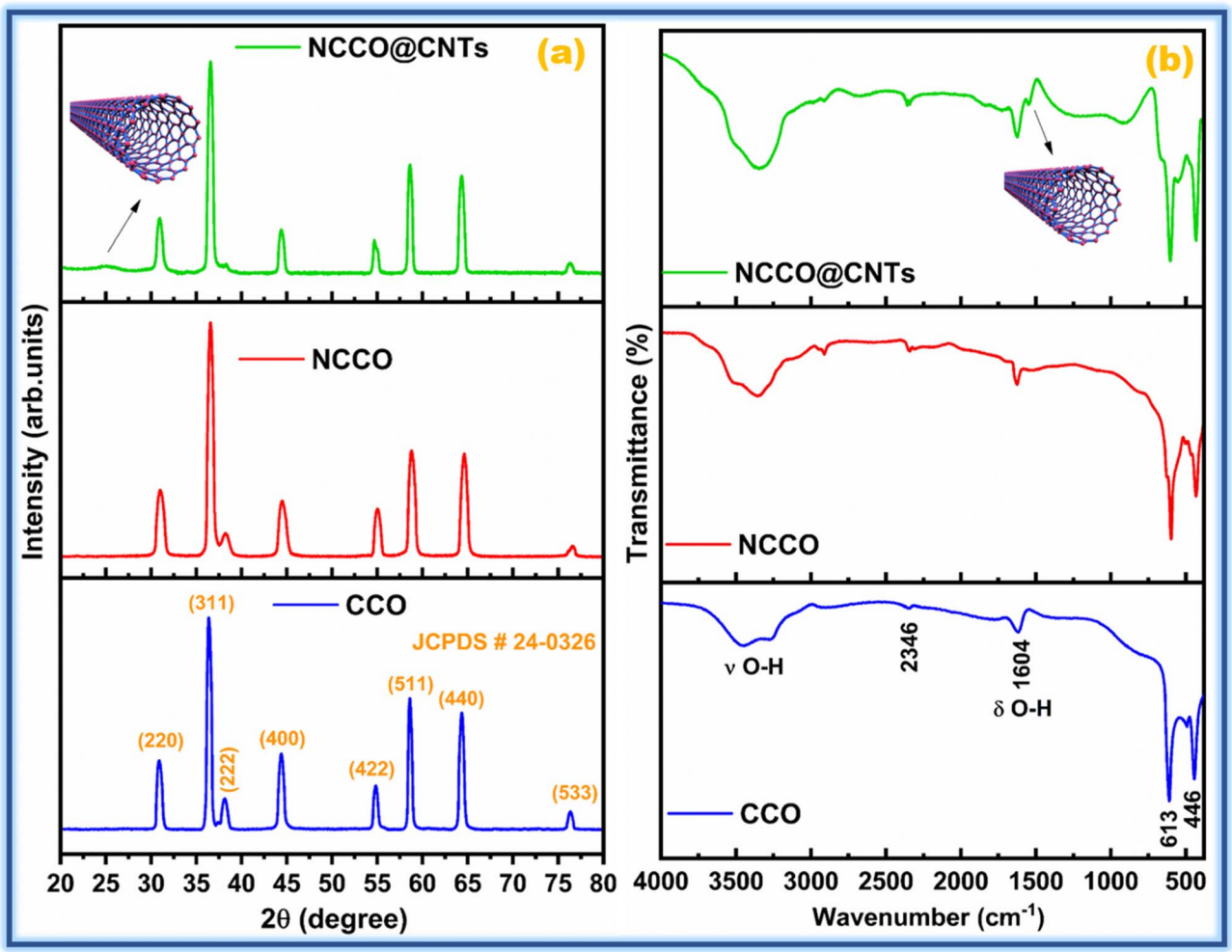

Fig. 2 (a) XRD and (b) FTIR of CCO, NCCO, and NCCO@CNTs.

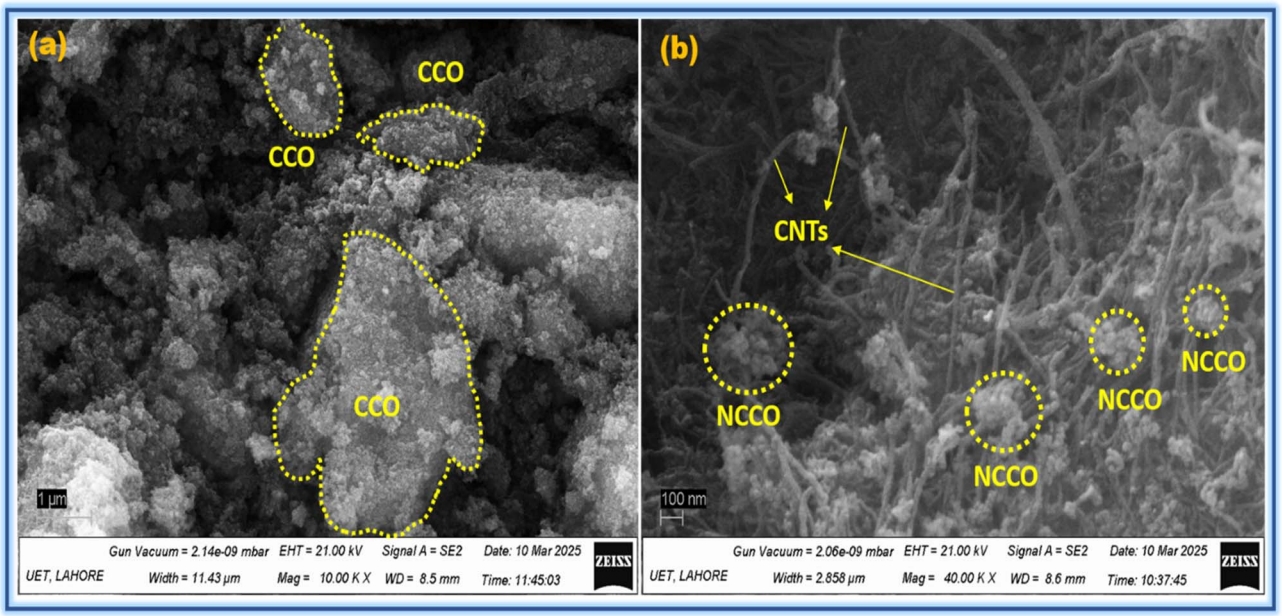

Fig. 3 SEM images of (a) CCO and (b) NCCO@CNTs.

lattice defects and quantum confinement effect upon the introduction of nitrogen. The domain/crystallite size was estimated by the Scherrer relation (eqn (3)).[25]

$$D = \frac{K\lambda}{\beta \cos \theta} \quad (3)$$

The average domain/crystallite size of CCO was 20.16 nm and that of NCCO was 16.19 nm, which again supported the findings of maximum peak broadening in case of NCCO. The NCCO@CNTs nanocomposites had an additional weak hump around 24–25° 2θ, which was caused by CNTs (absent in the XRD patterns of CCO or NCCO as individual materials). This peak and the presence of diffraction peaks for both NCCO and CNTs indicates that the synthesis of the NCCO@CNTs nanocomposite has been successful.

The typical FTIR spectra of the CCO, NCCO, and NCCO@CNTs, recorded using a Thermo Fisher Nicolet IS5, are shown in Fig. 2b, revealing a number of characteristic bands that can be used for the analysis of structural and bonding features in these materials. The transmittance bands of metal–oxygen (M–O) stretching vibrations occurring at octahedral and tetrahedral sites are identified in the CCO sample at 446 cm^{-1} and 613 cm^{-1}, respectively. These bands confirm the formation of a spinel-phase structure for CCO. The relatively weaker intensity of the band at 446 cm^{-1} compared to the 613 cm^{-1} band can be explained by the longer and weaker M–O bonds at the octahedral sites.[26] For the NCCO sample, these two bands redshift slightly. This trend suggests that the existence of structural defects or distortion from the doping nitrogen weakens the M–O bond.[27] NCCO@CNTs sample shows a full set of bands of NCCO and an extra weak band at 1500 cm^{-1} assigned to the C=C stretching vibration mode of the nanotubes (CNTs). The low intensity observed for this band can be explained by the non-polar character of the C=C bonds, thus negligible dipole moment alteration takes place during vibration.[28,29] Also, in case of all samples, a band at 1604 and 3445 cm^{-1} are observed that are attributed to the bending and stretching vibration of O–H groups, respectively.[30,31] These bands are assigned to the absorbed moisture of the samples. Moreover, one signal appearing at around 2346 cm^{-1} in all the samples is assigned to the asymmetric stretching vibration of O=C=O group related to absorbed CO_2.[32]

3.2 Morphological and elemental analysis

Fig. 3 displays the SEM images of CCO and NCCO@CNTs composite. The SEM images of the CCO sample (Fig. 3a) taken at ×10 000 indicate that the shape of particles is mostly aspherical and most of them are smaller than 100 nm in diameter.

However, larger micro-sized aggregates are also present on the CCO particles. Such bulky structures indicate an extent of agglomeration and may interfere with the dispersion of the material. The formation of bulky structures reduces the exposed surface area, consequently impeding the photocatalytic activity of the CCO material. These findings indicate that the agglomeration of the CCO particles limits their performance in photocatalytic applications, where surface interaction and the availability of active sites are critical. By contrast, the SEM image of the NCCO@CNTs using a higher magnification (×40 000), as shown in Fig. 3b, indicates that the particles are more spherical in shape and have better dispersions than those of the CCO sample.

The presence of CNTs in the matrix of NCCO is responsible for inhibiting the formation of large clusters. While a few minor clusters evidenced by the dashed circles are still visible, their size is considerably smaller than the domination clusters of the CCO sample. The NCCO particles interact well with the CNTs to

enable the inhibition of particle agglomeration and maintain good particle dispersion. This uniform dispersion enhances the available surface area and improves the material's photocatalytic performance. The NCCO particles have mostly filled the unevenly sized and shaped voids that were created by the random entanglement of the CNT particles. This not only makes the particles interact better, but it also stops them from sticking together on their own.

Energy-Dispersive X-ray Spectroscopy (EDX) analysis was conducted to verify the chemical structure and purity of the synthesized NCCO@CNTs composite. The EDS spectrum shown in Fig. 4a clearly identifies the presence of key elements: nitrogen (N), chromium (Cr), cobalt (Co), oxygen (O), and carbon (C), with a prominent C peak corresponding to the carbon nanotube (CNT) matrix integrated into the composite. The absence of any undesirable peaks further confirms the successful synthesis of the NCCO@CNTs composite and the chemical homogeneity of the hybrid material.

Fig. 4b–g are the elemental distribution maps of N, Cr, Co, O, and C showing a homogeneous and well-distributed incorporation of these elements into the composite structure. The distribution of these elements is important in ensuring the optimal transfer of charge and surface reactivity, which are major determinants of the increased photocatalytic activity of the material.[33] The addition of CNTs allows for better dispersion of the NCCO nanoparticles and allows for interactive interaction between the two materials, hence optimizing the photocatalytic activity for environmental purpose.

3.3 Optical and opto-electronic studies

The UV/Vis absorption spectra of CCO, NCCO, and NCCO@CNTs show clear distinctions in light absorption characteristics, affecting their photocatalytic performance. CCO absorbs light mainly below 400 nm (Fig. 5a), indicating a high bandgap and limiting its absorption to UV light.

On the other hand, the NCCO sample exhibits a redshift of the absorption edge to the visible region, which is contributed by the bandgap reduction arising from nitrogen doping. The absorption range of the composite is also broadened into visible wavelengths. CNTs instead improve the light absorption availability to the structure by increasing the material's spectral coverage and augmenting its light harvesting properties, especially in the visible region, originating from its black body nature.[32] By following the below given relation (eqn (4)),[34] the bandgap of CCO was 3.0 eV, whereas nitrogen doping reduced the bandgap of NCCO to 2.65 eV.

$$(\alpha h\nu)^{1/2} = A(h\nu - E_g) \quad (4)$$

This reduction facilitates better absorption of visible light, improving NCCO's photocatalytic performance by utilizing a wider range of the solar spectrum.[35] These results emphasize that nitrogen doping and CNT integration are effective approaches to enhance the light absorption and photocatalytic efficiency of $CrCo_2O_4$, making it suitable for environmental applications.

To examine the role of nitrogen doping and CNT incorporation in modulating possible charge separation, transient photocurrent profiles of CCO, NCCO, and NCCO@CNTs were recorded (Fig. 5b). The lowest photocurrent density was recorded for CCO. In contrast, N-doping resulted in a significant increase attributed to bandgap narrowing and the formation of shallow donor states, which improved the likelihood of photoexcitation. However, recombination within the spinel lattice continued to restrict carrier utilization.[33,36] A higher efficiency

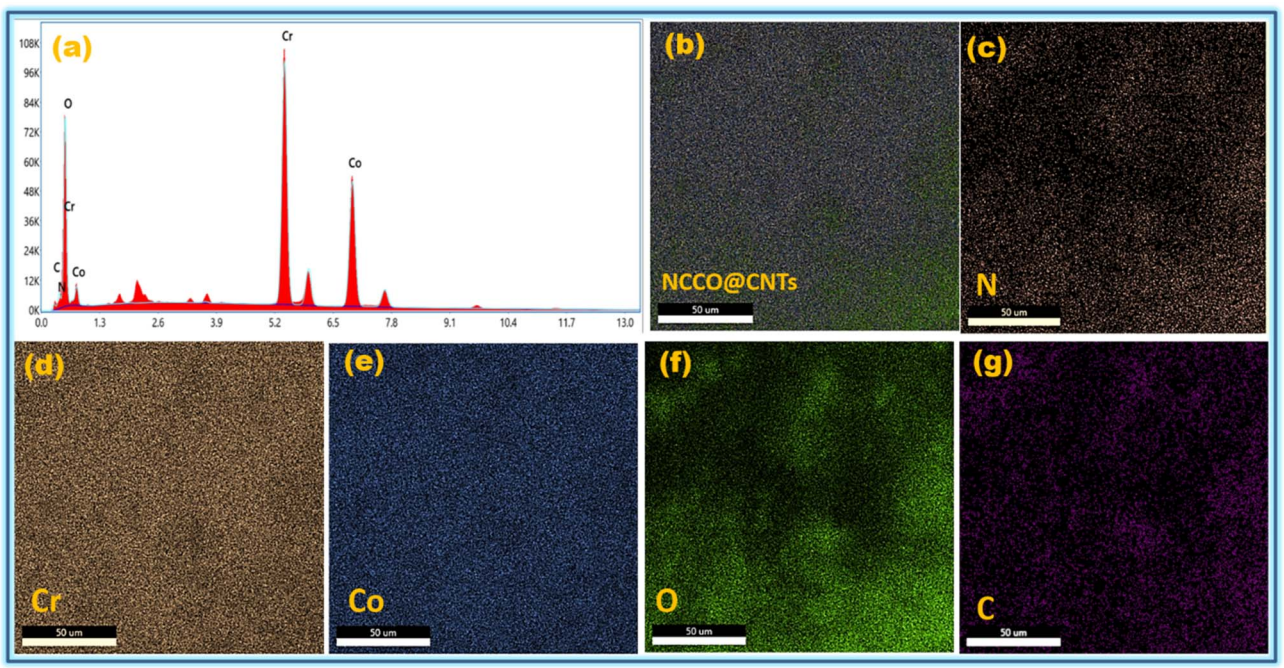

Fig. 4 (a) EDX spectrum of NCCO@CNTs, and (b–g) elemental mapping images confirming uniform distribution of N, Cr, Co, O and C.

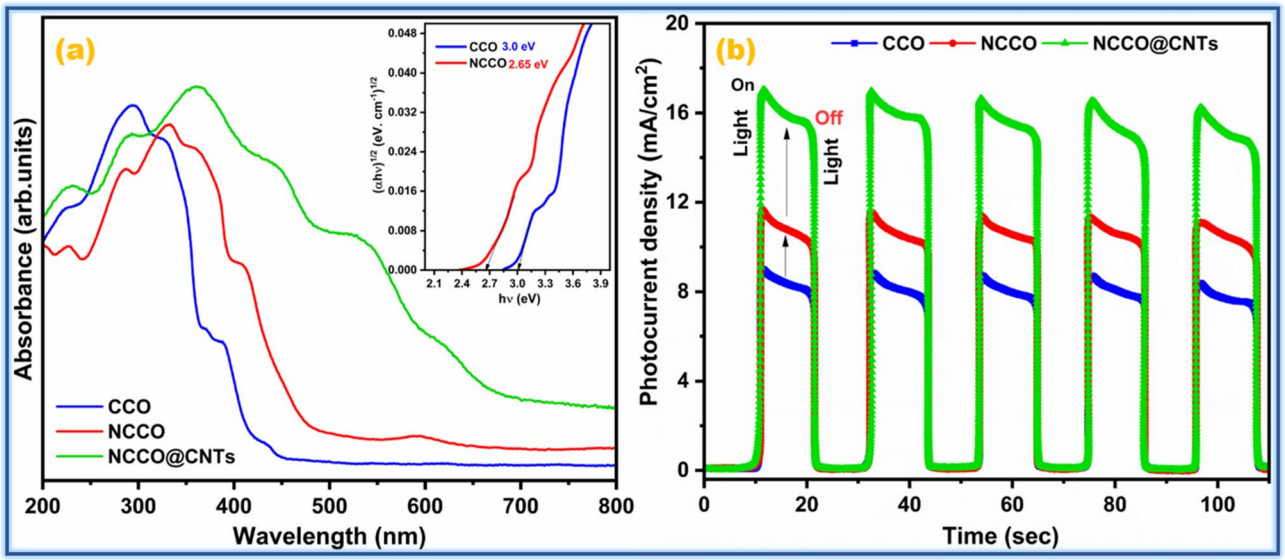

Fig. 5 (a) Optical absorption characteristics and (b) transient photocurrent response of CCO, NCCO, and NCCO@CNTs.

was obtained in the presence of CNTs, whose conductive network functioned as an active electron sink for promoting photoinduced NCCO to be extracted as soon as it is photoexcited and avoiding recombination, allowing an effective charge transport over longer distances toward the collector. The collaborative utilization of NCCO@CNTs leads to a higher photocurrent density compared to pristine CCO and NCCO.

3.4 Evaluation of photocatalytic activity

The photoactivity of CCO, NCCO, and NCCO@CNTs for the degradation of methylene blue (MB) dye was examined by time-dependent UV-Vis absorption spectra (Fig. 6a–c). The degradation was manifested as a pronounced decline in the intensity of the absorbance peak of MB at 665 nm. After 1 h sunlight exposure, CCO had the slowest degradation with a 49.5% reduction in MB dye (Fig. 6a). Then came NCCO, which degraded by 65.7% (Fig. 6b). The maximum MB degradation was achieved with the NCCO@CNTs composite, which degraded almost 90.7% MB dye during the same period of time (60 minutes) (Fig. 6c and d). The improvement in MB dye degradation from 49.5% (CCO) to 65.7% (NCCO) is principally due to N-doping. The introduction of N-dopant in the host's ($CrCo_2O_4$) lattice tuned the bandgap, which benefits the visible light absorption and possible charge separation, then promoting the degradation process.

The further enhancement in the MB dye degradation efficiency, that is from 65.7% (NCCO) to 90.7% (NCCO@CNTs), could be attributed to the incorporation of CNTs. Where CNTs greatly facilitate the charge collection, acting as the conductive networks and for suppressing recombination of electron–hole and providing a large surface area for adsorption of pollutants.[37,38] Both nitrogen doping and CNT introduction in NCCO@CNTs contribute to the best photocatalytic property and illustrate the synergy of these two modifications.

Based on the results of kinetic models applied to the degradation data, the selected kinetic model was pseudo-first-order kinetic, based on an R^2 value close to unity. The degradation of MB dye follows a pseudo-first-order kinetic pattern as seen in Fig. 6e and f, where NCCO@CNTs decay rate is the fastest. The rate constant (k) for CCO was 0.011 min^{-1}, increasing to 0.017 min^{-1} for NCCO and 0.037 min^{-1} for NCCO@CNTs, demonstrating a 3.36-fold enhancement over CCO. The enhanced efficiency can be explained by the synergistic effect of N doping and CNT reinforcement, which results in accelerated charge transfer, improved light harvesting ability, and an increase in surface reactive sites. In conclusion, a nitrogen-doped and CNT-loaded composite strongly enhances photocatalytic activity, leading to faster disappearance of MB dye in the presence of solar light.[39]

The photocatalytic degradation of amoxicillin over CCO, NCCO, and NCCO@CNTs was monitored by UV-Vis spectroscopy (Fig. 7a–c). The characteristic absorption band of amoxicillin at 230 nm gradually diminished with irradiation time, confirming its breakdown under solar light. After 60 min, the extent of removal followed the order NCCO@CNTs (85%) > NCCO (62%) > CCO (47.5%), as summarized in Fig. 7d.

Similar to the MB dye case, amoxicillin degradation improved step by step. Nitrogen doping upgrades the catalyst by narrowing the bandgap and stabilizing charge carriers. CNTs further enhance activity by making charge transport easier, reducing recombination, and expanding the reactive surface.[40]

The kinetic study (Fig. 7e and f) shows that amoxicillin degradation follows a pseudo-first-order reaction with an acceptable fit (R^2 = 0.99). The rate constant increased from 0.010 min^{-1} for CCO to 0.015 min^{-1} for NCCO and 0.030 min^{-1} for NCCO@CNTs, giving the composite nearly three times the activity of CCO due to faster charge transfer and less recombination.

Our results agree on one point: the modifications work, as both the faster kinetics and higher efficiencies point to the same conclusion-nitrogen doping improves light harvesting, and CNTs prevent recombination, together building a better

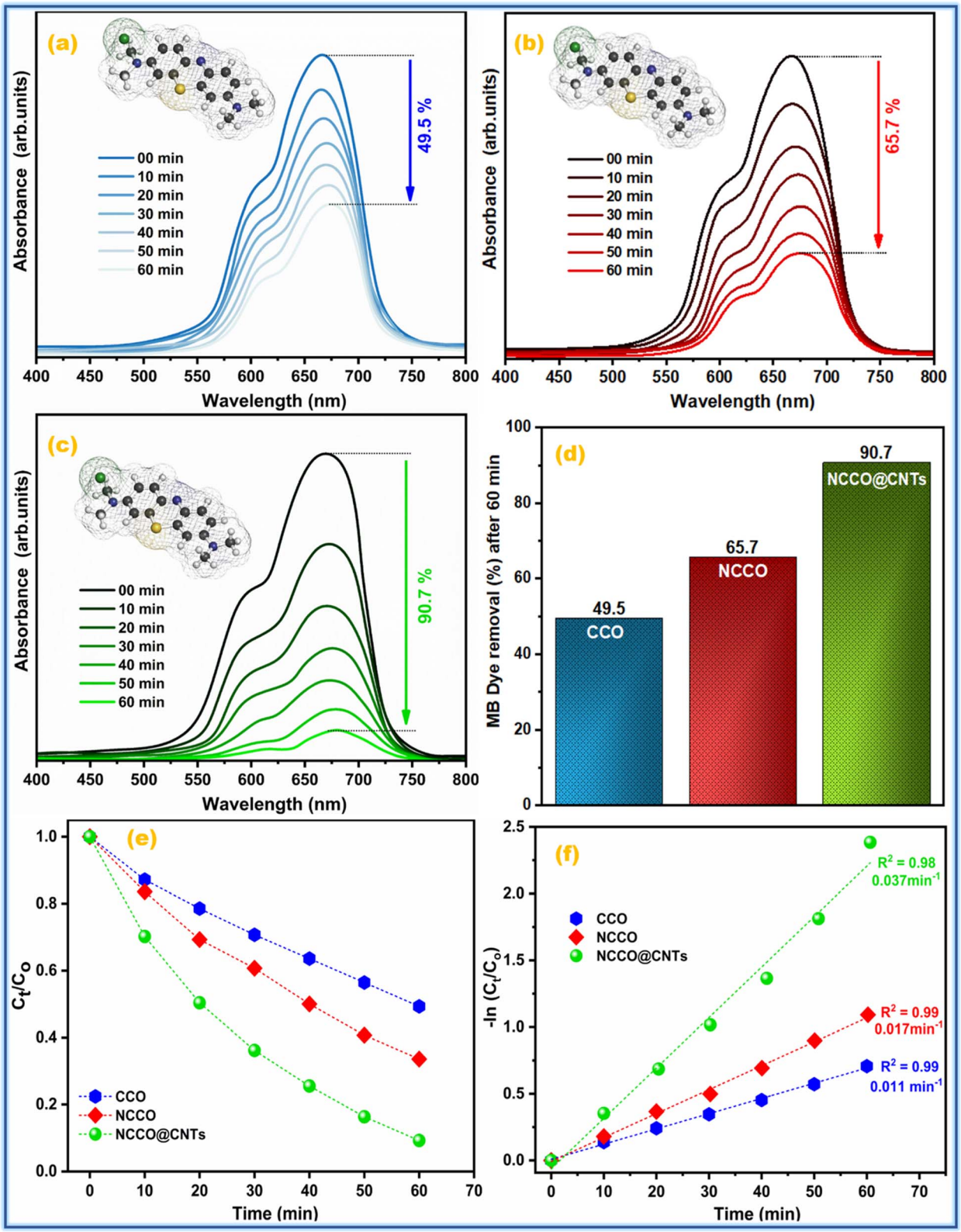

Fig. 6 Time-dependent UV-Vis spectra showing MB dye degradation over (a) CCO, (b) NCCO, and (c) NCCO@CNTs, (d) with corresponding degradation percentages and (e and f) kinetic analysis.

photocatalyst. Table 2 highlights this with side-by-side data for MB dye and amoxicillin, proving the strategy works for both dyes and pharmaceutical residues.

3.5 Trapping tests

To understand which reactive species, drive the photocatalytic process, we carried out scavenger tests with the most active

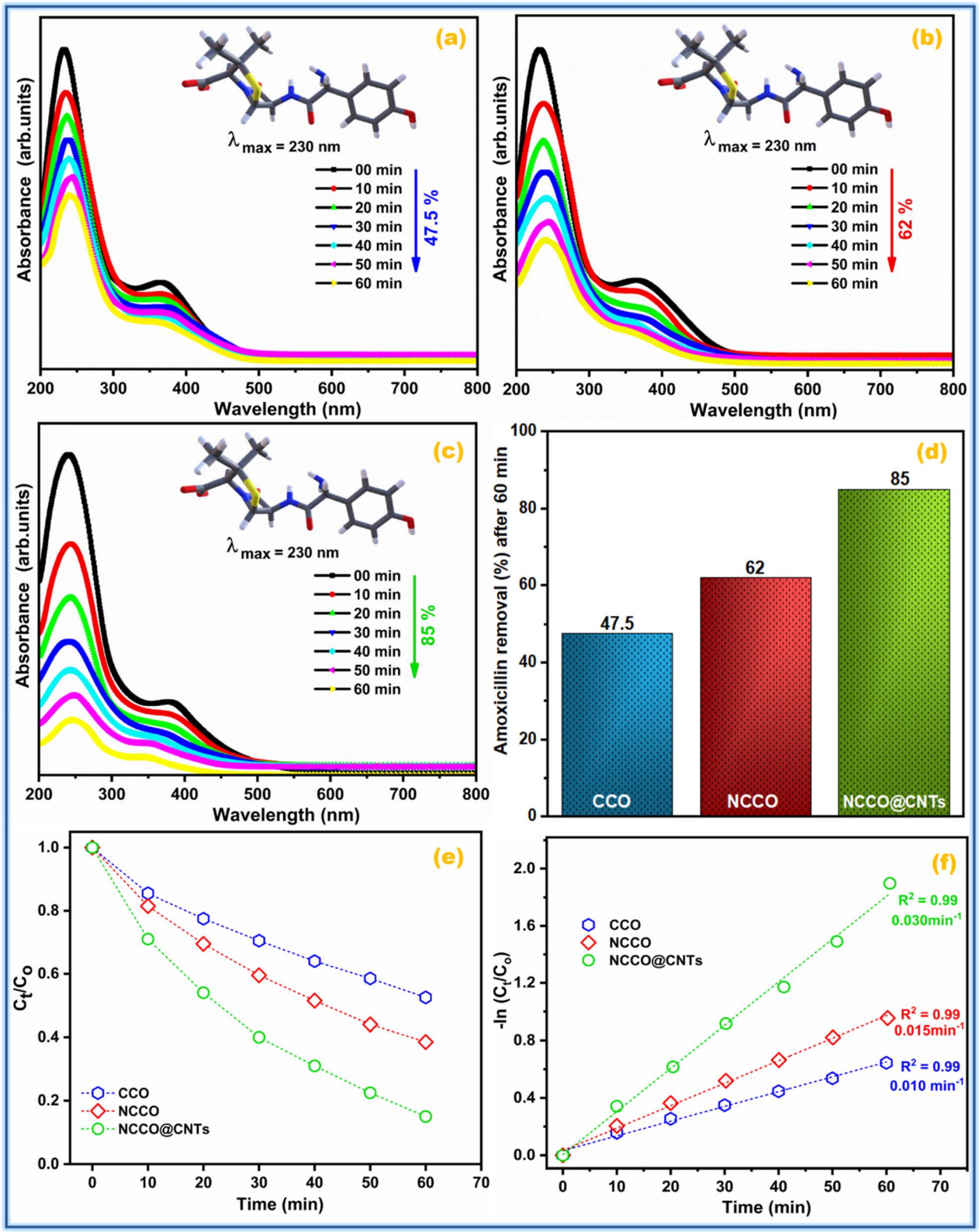

Fig. 7 Time-dependent UV-Vis spectra showing AMX degradation over (a) CCO, (b) NCCO, and (c) NCCO@CNTs, (d) with corresponding degradation percentages and (e and f) kinetic analysis.

catalyst (NCCO@CNTs). Different chemical quenchers were added: $AgNO_3$ to trap electrons (e^-), EDTA for holes (h^+), *p*-benzoquinone (*P*-BQ) for superoxide radicals ($O_2^{\bullet -}$), and 2-propanol for hydroxyl radicals ($^{\bullet}OH$).[41] Their effects on the degradation of MB dye and amoxicillin are presented in Fig. 8a–d.

Table 2 Comprehensive analysis of methylene blue and amoxicillin degradation parameters in the presence of various photocatalysts

S. no.	Photocatalyst	Pollutant	Light source	% Degradation	Rate constant (min^{-1})
1	CCO	Methylene blue	Sunlight	49.5	0.011
2	NCCO	Methylene blue	Sunlight	65.7	0.017
3	NCCO@CNTs	Methylene blue	Sunlight	90.7	0.037
4	CCO	Amoxicillin	Sunlight	47.5	0.010
5	NCCO	Amoxicillin	Sunlight	62	0.015
6	NCCO@CNTs	Amoxicillin	Sunlight	85	0.030

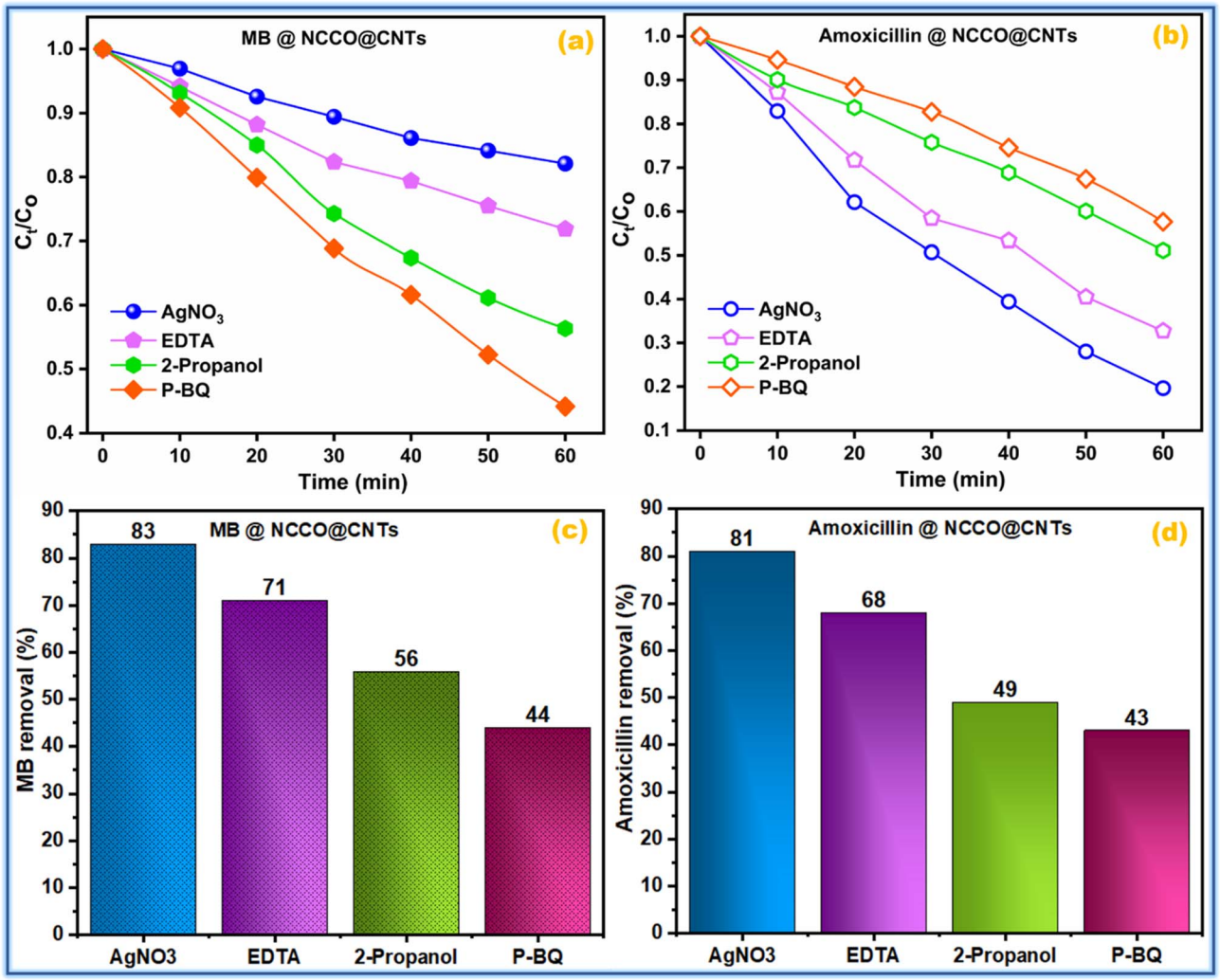

Fig. 8 Effect of different radical scavengers on the photocatalytic degradation of (a) MB dye and (b) amoxicillin over NCCO@CNTs, and (c and d) compare the corresponding degradation efficiencies.

The MB dye removal efficiency (Fig. 8a and c) dropped from 90.7% to 83% ($AgNO_3$), 71% (EDTA), 56% (2-propanol), and 44% (*P*-BQ). This pattern shows superoxide radicals are the most decisive factor, hydroxyl radicals and holes have a strong effect too, and electrons are the least involved. As seen in Fig. 8b and d, amoxicillin degradation followed the same order of scavenger effects: 81% ($AgNO_3$), 68% (EDTA), 49% (2-propanol), and only 43% (*P*-BQ).

The major influence of *P*-BQ and 2-propanol highlights that superoxide and hydroxyl radicals are the key species, while the rest contribute less. Since *P*-BQ and 2-propanol caused the biggest drop-in activity, we know superoxide and hydroxyl radicals are the central species in this reaction. For a fair comparison, Table 3 presents our results alongside those of other spinel oxide photocatalysts, highlighting the relative performance of our material.

Table 3 Evaluation of photocatalytic activity in reported spinel oxides *versus* findings from the current study

S. no.	Photocatalysts	Pollutant	Light source	Degradation (%)	References
1	$ZnCo_2O_4$	Methylene blue	Sunlight	41.97	42
2	$Ag–ZnCo_2O_4$	Methylene blue	Sunlight	58.02	42
3	$ZnCo_2O_4$	Crystal violet	Tungsten bulb	61.6	43
4	$CuO/ZnCo_2O_4$	Crystal violet	Tungsten bulb	78	43
5	$CuO/ZnCo_2O_4$/CNTs	Crystal violet	Tungsten bulb	87.7	43
6	$NiCo_2O_4$	Methyl red	Visible light	95.1	44
7	$NiCo_2O_4/gC_3N_4$	Congo red	Solar light	65	45
8	$NiCo_2O_4/gC_3N_4$	Rhodamine B	Solar light	50	45
9	$N–CrCo_2O_4$@CNTs	Methylene blue	Sunlight	90.7	Current work
10	$N–CrCo_2O_4$@CNTs	Amoxicillin	Sunlight	85	Current work

3.6 Degradation mechanism

Mechanism of photocatalytic degradation over NCCO@CNTs, shown in Fig. 9, demonstrates that: photon-induced excitation creates electrons and holes that participate in oxidative and reductive reactions, destroying pollutants. The positions of the conduction band (E_{CB}) and valence band (E_{VB}) are estimated using a standard formula that involves the semiconductor's absolute electronegativity (χ), the energy of free electrons on the hydrogen scale (commonly taken as 4.5 eV), and the optical bandgap (E_g) of the material:

$$E_{VB} = \chi - E_e + 0.5E_g \quad (5)$$

$$E_{CB} = E_{VB} - E_g \quad (6)$$

The mechanism of the composite-driven degradation is proposed as visible-light excites NCCO *via* photons with energy matching or exceeding its bandgap. This process moves electrons up into the conduction band, leaving holes in the valence band. The E_{VB} is sufficiently positive (2.775 *vs.* NHE) to facilitate the oxidation of both water and hydroxide ions into highly reactive hydroxyl free radicals. Hydroxyl free radicals, being several times more reactive than simple holes, attack the pollutant molecules and degrade them. The conduction band (CB) potential by itself is not sufficiently negative (0.125 *vs.* NHE) to reduce oxygen directly into superoxide radicals ($^{\bullet}O_2^-$).[46,47]

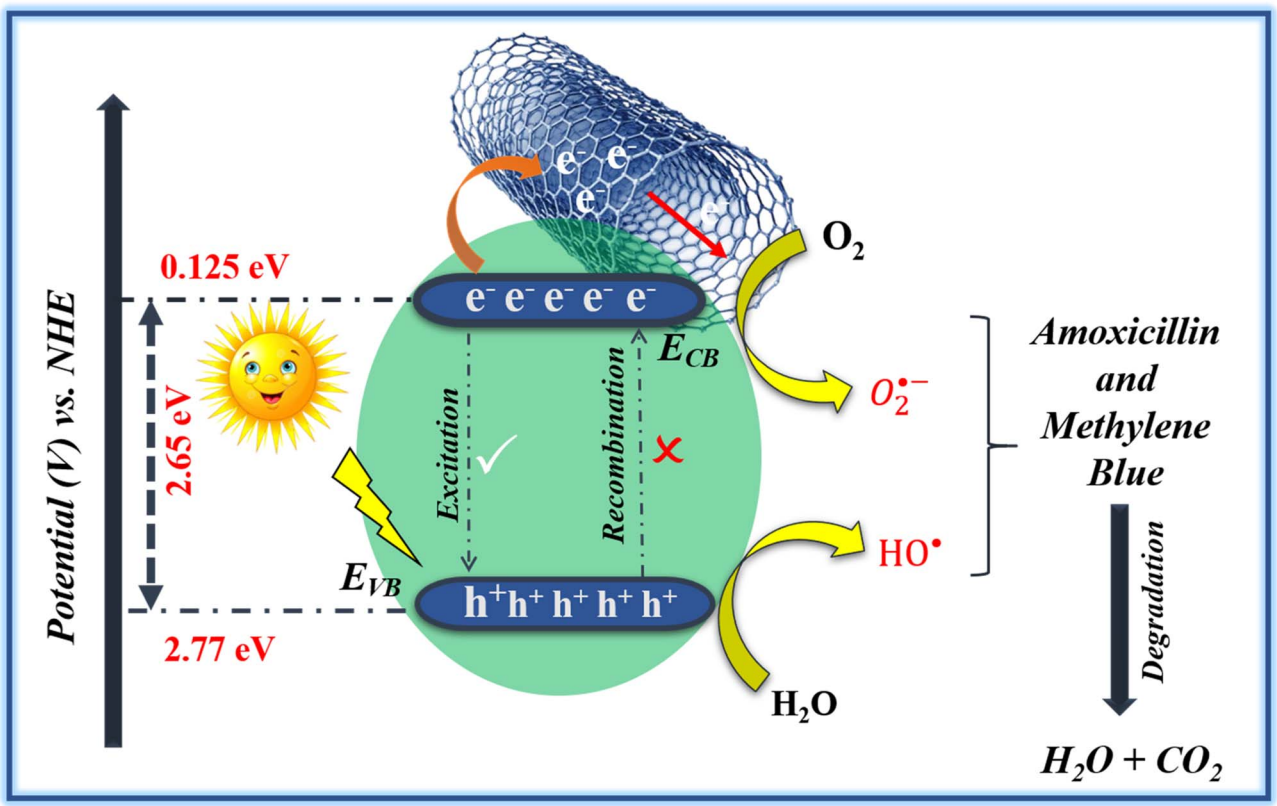

Fig. 9 Schematic of the charge-transfer and reactive species pathways in the photocatalytic degradation of pollutants by NCCO@CNTs.

CNTs play a helpful role at this point through immediate acceptance of the excited electrons, eliminating the chances of their recombination and stabilizing them long enough to transfer to O_2 molecules. This transfer of electrons to oxygen forms $^{\bullet}O_2^-$. The hydroxyl and superoxide radicals have a synergistic effect to degrade pollutants. VB hole oxidizes water or hydroxide for $^{\bullet}OH$ formation. CNTs stabilize and donate an electron to oxygen for $^{\bullet}O_2^-$ creation. The two radicals work together to quickly and efficiently degrade the pollutant molecules-degrading drugs and dyes-into harmless mineralized forms.

4. Conclusion

Nanotechnology, nitrogen doping, and the formation of CNT-based composites are effective methods for improving the photocatalytic activity of spinel-type chromium cobaltite ($CrCo_2O_4$). This study demonstrates this point. The wet-chemical precipitation method was employed to synthesize the catalysts, with nitrogen introduced through urea doping and CNTs added through ultrasonication to guarantee uniform dispersion. The synthesis was effective, and the modified materials exhibited superior charge transport characteristics, as demonstrated by comprehensive testing. Nitrogen doping resulted in a 65.7% and 62% increase in the degradation of methylene blue (49.5%) and amoxicillin (47.5%) in pristine CCO, as demonstrated by photocatalytic experiments. NCCO@CNTs exhibited the highest activity, with a 90.7% degradation of methylene blue and 85% of amoxicillin, as well as the highest kinetic rate constants. The enhancements are derived from nitrogen doping, which reduces recombination, adds active sites, and improves light absorption by narrowing the bandgap. Additionally, CNTs are used to trap electrons. The most prevalent reactive species involved in the degradation process were hydroxyl ($^{\bullet}OH$) and superoxide ($^{\bullet}O_2^-$) radicals, as confirmed by scavenger assays. Presently, the combination of doping and the formation of CNT composite greatly improved the efficiency of $CrCo_2O_4$ for the removal of pollutants. The robust activity against both dyes and pharmaceutical pollutants demonstrate the promise of NCCO@CNTs as a scalable photocatalyst for wastewater treatment and more extensive environmental remediation.

Author contributions

Mohamed Abdel Rafea: methodology, funding acquisition, and resources. Kashif Ali: visualization. Mohamed I. Attia: data curation, formal analysis. M. M. Rashed: project administration, conceptualization. Mohamed R. El-Aassar: writing – original draft, data curation, formal analysis. Imran Shakir: conceptualization. Abdullah K. Alanazi: writing – review & editing. Sidra Mubeen: writing – co-supervision. Muhammad Aadil: supervision.

Conflicts of interest

There are no conflicts to declare.

Data availability

Data will be available upon request.

Acknowledgements

This work was supported and funded by the Deanship of Scientific Research at Imam Mohammad Ibn Saud Islamic University (IMSIU) (grant number IMSIU-DDRSP2602).

References

1 Z. H. Jabbar and B. H. Graimed, Recent developments in industrial organic degradation via semiconductor heterojunctions and the parameters affecting the photocatalytic process: A review study, *J. Water Process Eng.*, 2022, **47**, 102671.
2 M. Hambi, M. Khadraoui, R. Miloua, A. Bouzidi, A. Nakrela, M. Medles and Z. Amara, Structural evolution and photocatalytic performance of ZnS–ZnO thin films synthesized by spray pyrolysis, *Ceram. Int.*, 2024, **50**, 35902–35914.
3 J. Chen, Y. Chen, J. Shuai, X. Chen, D. Zhang, X. Lu, X. Fang, B. Zou, X. Yu and F. Zhao, Enhancement of visible light adsorption and photocatalytic degradation activity of organic dye by coating semiconducting TiO_2 shell on plasmonic Au particles, *J. Alloys Compd.*, 2024, **1009**, 176938.
4 M. F. Lanjwani, M. Tuzen, M. Y. Khuhawar and T. A. Saleh, Trends in photocatalytic degradation of organic dye pollutants using nanoparticles: A review, *Inorg. Chem. Commun.*, 2024, **159**, 111613.
5 W. Zhang, F. Zhao, J. Han, J. Wu, X. Nie, Z. Wang, Z. Dong and L. Huang, Preparation of polyetherimide/Bi_2MoO_6 composite membrane by electrospinning and hydrothermal method for rapid photocatalysis and its degradation mechanism, *J. Water Process Eng.*, 2025, **78**, 108681.
6 A. Saberyoun, A. Fattah-alhosseini, M. Karbasi, R. Hosseini and M. Kaseem, Boosting the visible-light-driven photocatalytic efficiency in porous Cu/TiO_2 ceramic coatings, *Ceram. Int.*, 2024, **50**, 31313–31325.
7 J. Fang, K. Wang, P. Chen, X. Xu, C. Zhang, Y. Wu, Y. Yan and Z. Zuo, Oxidation of soot by cerium dioxide synthesized under different hydrothermal conditions, *Molecules*, 2025, **30**, 1161.
8 F. Khan, M. S. Khan, S. Kamal, M. Arshad, S. I. Ahmad and S. A. Nami, Recent advances in graphene oxide and reduced graphene oxide based nanocomposites for the photodegradation of dyes, *J. Mater. Chem. C*, 2020, **8**, 15940–15955.
9 X. He, M. Wang and L. Li, Characterization and photocatalytic properties of porous ZrO_2/Al_2O_3 ceramic bead supported BiOI catalyst, *Ceram. Int.*, 2024, **50**, 12529–12538.
10 I. J. Budiarso, V. A. Dabur, R. Rachmantyo, H. Judawisastra, C. Hu and A. Wibowo, Carbon nitride-and graphene-based

materials for the photocatalytic degradation of emerging water pollutants, *Mater. Adv.*, 2024, **5**, 2668–2688.
11 Y. Li, Y. Li, B.-J. Ni, Y.-Z. Li and S.-Q. Ni, Towards scalable anammox: mechanistic insights and emerging strategies, *Trends Biotechnol.*, 2025, DOI: 10.1016/j.tibtech.2025.08.013.
12 Z. Cui, R. Yuan, H. Chen, B. Zhou, B. Zhu and C. Zhang, Application of polyaniline-based photocatalyst in photocatalytic degradation of micropollutants in water: A review, *J. Water Process Eng.*, 2024, **59**, 104900.
13 D. Bouras, M. Fellah, A. Mecif, R. Barillé, A. Obrosov and M. Rasheed, High photocatalytic capacity of porous ceramic-based powder doped with MgO, *J. Korean Ceram. Soc.*, 2023, **60**, 155–168.
14 H.-T. Vuong, T. Mahvelati-Shamsabadi, T. T. Dang, S. H. Hur and J. S. Chung, EDTA linker for S-scheme CdS/spinel oxides heterojunction photocatalyst for visible-light-driven hydrogen production, *Korean J. Chem. Eng.*, 2024, **41**, 309–323.
15 L. Zhang, S. Xia, X. Zhang, Y. Yao, Y. Zhang, S. Chen, Y. Chen and J. Yan, Low-temperature synthesis of mesoporous half-metallic high-entropy spinel oxide nanofibers for photocatalytic CO_2 reduction, *ACS Nano*, 2024, **18**, 5322–5334.
16 A. M. Fallatah, S. Aman and H. M. T. Farid, Facile hydrothermally synthesized 2D-based rGO/NiO nanohybrid for environmental remediation of malachite green pollutant, *Korean J. Chem. Eng.*, 2024, **41**, 503–513.
17 A. Razzaq, A. Kumar, A. M. Afzal, B. Kanabar, S. Ballal, M. Alsabah, K. Jayabalan, S. Samantaray, H. Karamti and S. Kaushal, Design and characterization of Co-MOF/$CrCo_2O_4$ nanocomposites on carbon paper electrode for supercapacitors and biosensor applications, *J. Mater. Sci.: Mater. Electron.*, 2025, **36**, 1578.
18 F. M. A. Alzahrani, M. Anwar, A. Farooq, Z. Alrowaili, M. Al-Buriahi and M. F. Warsi, A new BiOCl–$ZnFe_2O_4$/CNTs ternary composite for remarkable photocatalytic degradation studies of a herbicide and a diazo dye, *Opt. Mater.*, 2024, **148**, 114876.
19 K. M. Katubi, A. Murtaza, H. M. Asif, Z. Alrowaili, M. Al-Buriahi, S. Munir and M. F. Warsi, Fabrication and characterization of ternary composite $MgFe_2O_4$/MoO_3@CNTs for the enhanced photocatalytic activity to degrade organic pollutants, *J. Alloys Compd.*, 2024, **978**, 173327.
20 C. Sun, J. Lu, F. Rao, Y. Sun, J. Ye, S. Gong, Q.-U. Hassan, S. M. Zubairu, L. Zhu and Y. An, Highly efficient and selective NO photocatalytic abatement by tuning charge separation in multi-walled carbon nanotubes and Bi_2WO_6 microsphere heterojunction, *Surf. Interfaces*, 2024, **51**, 104806.
21 A. Moin, K. M. Younes, U. Fatima, S. M. D. Rizvi, A. S. A. Lila, A. A. AL-Shammary and M. F. Warsi, A mechanistic investigation of $Mg_xZn_{1-x}FeO_3$/CNTs nanocomposite for photocatalytic degradation of rhodamine b and acetaminophen, *J. Alloys Compd.*, 2025, **1020**, 179274.
22 M. Ishfaq, M. Aadil, S. R. Ejaz, W. Hassan, N. M. Panduro-Tenazoa, M. E. El Sayed, M. N. Murshed and Z. M. El-Bahy, Synthesis of binary metal doped CeO_2 via the subcritical hydrothermal method for photo-mineralizing methyl orange dye, *J. Alloys Compd.*, 2023, **960**, 170661.
23 M. Sabir, M. Ramzan, M. Imran, S. R. Ejaz, A. Anwar, S. Ahmad, M. Aamir and M. Aadil, Synthesis of $La_{1-x}Gd_xFe_{1-y}Co_yO_3$/r-GO nanocomposite with integrated features for the treatment of hazardous industrial effluents, *Ceram. Int.*, 2022, **48**, 9134–9145.
24 A. Saad, H. Shen, Z. Cheng, Q. Ju, H. Guo, M. Munir, A. Turak, J. Wang and M. Yang, Three-dimensional mesoporous phosphide–spinel oxide heterojunctions with dual function as catalysts for overall water splitting, *ACS Appl. Energy Mater.*, 2020, **3**, 1684–1693.
25 K. Zafar, M. Aadil, M. N. Shahi, H. Sabeeh, M. F. Nazar, M. Iqbal and M. A. Yousuf, Physical, structural and dielectric parameters evaluation of new $Mg_{1-x}Co_xNiyFe_{2-y}O_4$ nano-ferrites synthesized via wet chemical approach, *AAAFM Energy*, 2020, **1**, 36–44.
26 A. Ahmad, S. Khan, M. S. Javed, S. Osman, H. Li, S. Majeed and R. Luque, Improved electrochemical performance of aqueous hybrid supercapacitors using $CrCo_2O_4$ mesoporous nanowires: an innovative strategy toward sustainable energy devices, *ACS Appl. Mater. Interfaces*, 2024, **16**, 6920–6930.
27 K. Shafiq, M. Aadil, W. Hassan, Q. Choudhry, S. Gul, A. Rais, A. A. Fattah, K. H. Mahmoud and M. Z. Ansari, Cobalt and holmium co-doped nickel ferrite nanoparticles: synthesis, characterization and photocatalytic application studies, *Z. Phys. Chem.*, 2023, **237**, 1325–1344.
28 M. S. Taleghani, N. S. Tabrizi and P. Sangpour, Enhanced visible-light photocatalytic activity of titanium dioxide doped CNT-C aerogel, *Chem. Eng. Res. Des.*, 2022, **179**, 162–174.
29 E. Valadez-Rentería, R. Pérez-González, C. Gómez-Solís, L. A. Díaz-Torres, A. Encinas, J. Oliva and V. Rodríguez-González, A novel and stretchable carbon-nanotube/Ni@TiO_2: W photocatalytic composite for the complete removal of diclofenac drug from the drinking water, *J. Environ. Sci.*, 2023, **126**, 575–589.
30 M. O. Yusuf, Bond characterization in cementitious material binders using Fourier-transform infrared spectroscopy, *Appl. Sci.*, 2023, **13**, 3353.
31 Y. Wang, B. Tian, Y. Tian, W. Wang, X. Ma, Y. Liu and J. Hou, Orbital Hybridization-Mediated Decoupling of Electrocatalytic Functions for Paired CO_2 Electrosynthesis, *Adv. Sci.*, 2026, e22711.
32 M. Elavarasan, W. Yang, S. Velmurugan, J.-N. Chen, T. C.-K. Yang and T. Yokoi, Highly efficient photothermal reduction of CO_2 on Pd_2Cu dispersed TiO_2 photocatalyst and operando DRIFT spectroscopic analysis of reactive intermediates, *Nanomaterials*, 2022, **12**, 332.
33 T. A. Nguyen, V. Pham, T. L. Pham, L. T. T. Nguyen, I. Y. Mittova, V. Mittova, L. N. Vo, B. T. T. Nguyen, V. X. Bui and E. Viryutina, Simple synthesis of $NdFeO_3$ nanoparticles by the co-precipitation method based on a study of thermal behaviors of Fe (III) and Nd (III) hydroxides, *Crystals*, 2020, **10**, 219.

34 H. A. Alburaih, M. Aadil, S. R. Ejaz, W. Hassan, A. Anwar, S. Anjum, S. Aman, M. S. Al-Buriahi, Z. A. Alrowaili and A. V. Trukhanov, Wet-chemical synthesis of urchin-like Co-doped CuO: A visible light trigger photocatalyst for water remediation and antimicrobial applications, *Ceram. Int.*, 2022, **48**, 21763–21772.

35 H. Baqiah, N. Zhang, M. M. A. Kechik, N. M. Al-Hada, S. K. Tiong, A. A. Al-Zahrani, J. Liu, Q. Li and S. Xu, Crystal growth, optical, photoluminescence and magnetic properties of sol-gel $GdFeO_3$ thin film, *Ceram. Int.*, 2024, **50**, 13892–13900.

36 J. Louis, N. T. Padmanabhan, M. K. Jayaraj and H. John, Exploring enhanced interfacial charge separation in ZnO/reduced graphene oxide hybrids on alkaline photoelectrochemical water splitting and photocatalytic pollutant degradation, *Mater. Res. Bull.*, 2024, **169**, 112542.

37 J. Naseem, M. A. Rafea, M. E. Zaki, M. I. Attia, M. R. El-Aassar, F. Alresheedi, S. Zulfiqar and M. Aadil, Combining nanotechnology and nanohybrid methods to improve the physical and chemical properties of CuS and boost its photocatalytic aptitude, *RSC Adv.*, 2025, **15**, 13940–13950.

38 M. Dagar, S. Kumar, A. Jain, A. Vohra, M. Singh, J. Dalal, S. Kumar and S. Kaushal, Synergistic Ce/Ag/N-doped ZnO–MWCNT nanocomposites for efficient photocatalytic wastewater remediation with visible light, *Mater. Adv.*, 2025, **6**, 4522–4537.

39 M. A. Ahmed, S. A. Mahmoud and A. A. Mohamed, Interfacially engineered metal oxide nanocomposites for enhanced photocatalytic degradation of pollutants and energy applications, *RSC Adv.*, 2025, **15**, 15561–15603.

40 P. Sun, S. Zhou, Y. Yang, S. Liu, Q. Cao, Y. Wang, T. Wågberg and G. Hu, Artificial chloroplast-like phosphotungstic acid—iron oxide microbox heterojunctions penetrated by carbon nanotubes for solar photocatalytic degradation of tetracycline antibiotics in wastewater, *Adv. Compos. Hybrid Mater.*, 2022, **5**, 3158–3175.

41 Y. Li, Z. Wang, H. Zhao and M. Yang, Composite of TiO_2 nanoparticles and carbon nanotubes loaded on poly (methyl methacrylate) nanofibers: Preparation and photocatalytic performance, *Synth. Met.*, 2020, **269**, 116529.

42 H. M. Abo-Dief, S. M. El-Bahy, O. K. Hussein, Z. M. El-Bahy, M. Shahid and I. Shakir, Synthesis and characterization of rGO supported silver doped bimetallic $ZnCo_2O_4$ spinel oxides for enhanced photocatalytic degradation of industrial effluents, *J. Alloys Compd.*, 2022, **913**, 165164.

43 N. Alomayrah, M. Ikram, S. Zulfiqar, S. Alomairy, M. S. Al-Buriahi, I. Shakir, M. F. Warsi and E. W. Cochran, Fabrication of a highly efficient $CuO/ZnCo_2O_4$/CNTs ternary composite for photocatalytic degradation of hazardous pollutants, *RSC Adv.*, 2024, **14**, 24874–24897.

44 Y. Wan, J. Chen, J. Zhan and Y. Ma, Facile synthesis of mesoporous $NiCo_2O_4$ fibers with enhanced photocatalytic performance for the degradation of methyl red under visible light irradiation, *J. Environ. Chem. Eng.*, 2018, **6**, 6079–6087.

45 A. Naz, I. Bibi, F. Majid, A. Dahshan, K. Jilani, B. Taj, A. Ghafoor, Z. Nazeer, F. M. Alzahrani and M. Iqbal, Cu and Fe doped $NiCo_2O_4$/g-C_3N_4 nanocomposite ferroelectric, magnetic, dielectric and optical properties: Visible light-driven photocatalytic degradation of RhB and CR dyes, *Diamond Relat. Mater.*, 2024, **141**, 110592.

46 W. S. Koe, J. W. Lee, W. C. Chong, Y. L. Pang and L. C. Sim, An overview of photocatalytic degradation: photocatalysts, mechanisms, and development of photocatalytic membrane, *Environ. Sci. Pollut. Res.*, 2020, **27**, 2522–2565.

47 H. D. Tran, D. Q. Nguyen, P. T. Do and U. N. Tran, Kinetics of photocatalytic degradation of organic compounds: a mini-review and new approach, *RSC Adv.*, 2023, **13**, 16915–16925.